Eur. Phys. J. D **12**, 355–367 (2000)

THE EUROPEAN PHYSICAL JOURNAL D

EDP Sciences

Asymmetry of Stark profiles

The microfield point of view

C. Stehlé[1,a], D. Gilles[2,b], and A.V. Demura[3,c]

[1] DASGAL[d], Observatoire de Paris, 5 place J. Janssen, 92195 Meudon, France
[2] CEA, Ile-de-France, B.P. 12, 91680 Bruyères le Châtel Cedex, France
[3] Hydrogen Energy and Plasma Technology Institute, Russian Research Center Kurchatov Institute, Moscow 123182, Russia

Received 21 January 2000 and Received in final form 27 April 2000

Abstract. The theoretical basis is presented that allows to compute the Stark broadened line shapes of atomic ions up to the quadrupole terms in the interaction potential between the radiator and the plasma electric microfields and their gradients. The nature of the corrections due to the *plasma polarization effects associated with the electron distribution around ion perturbers* are carefully analyzed. The relevant universal plasma functions are evaluated in a cluster expansion or by Monte Carlo simulations, and the line shape is calculated with ion dynamic effects by the Model Microfield Method. The asymmetry of the Lyman α line of hydrogenic ions is then studied.

PACS. 32.70.Jz Line shapes, widths, and shifts – 95.30.-k Fundamental aspect of astrophysics – 95.30.Dr Atomic processes and interactions

1 Introduction

The spectral lines of hydrogen-like radiators immersed in plasmas show noticeable asymmetry and often measurable shifts at high densities [1–27]. This reflects the fundamental properties of hydrogen-like radiators as a tiny quantum-mechanical probes of the plasma-radiator interaction. The understanding of these properties provides the basis of sensitive spectroscopic diagnostics for experimental studies, for example, ICF [7,8]. In a first approximation, the line shapes of transitions in hydrogen and hydrogenic ions are due to the interaction between the bound electron and the plasma electric microfield, leading to symmetric linear Stark energy splitting of the degenerate parabolic eigenstates (n, n_1, n_2, m). Thus the line shapes are symmetrical around the line center. An intrinsic source of the line asymmetry in the absence of any external perturbation is due to the fine structure effects. Another asymmetry is observed when plasma density is increasing. Depending on the plasma parameters this asymmetry in the profile can be attributed to several sources like high-order terms in the multipole expansion of the radiator-plasma interaction potential (quadrupole terms, quadratic Stark effect etc.), Boltzmann factors *versus* the detuning from the line center, dielectronic satellites, differences in the field ionization rates and electronic collision shifts of the symmetrically split Stark components [9,10,15].

The theoretical estimation of the contribution from ion quadrupole effects has changed many times [9,15]. Recently, the quantum mechanical calculations of the electronic shifts and line asymmetry of hydrogenic lines using the Green-function technique [19,20], indicate the dominant contribution of the quadrupole effects in the case of Balmer lines. However, the inclusion of quadratic Stark effect in the whole series of papers [19–22] was performed inconsistently[1].

The line shape asymmetry in plasmas, which is associated with the quadrupole contribution induced by the electron-radiator and ion-radiator interaction, is mainly due to differences in the electron-radiator and ion-radiator interactions, which have opposite signs. First, the spatial distributions of the plasma electrons and ions in the vicinity of a charged radiator differ strongly (leading

[a] e-mail: Chantal.Stehle@obspm.fr
[b] e-mail: Dominique.Gilles@bruyeres.cea.fr
[c] e-mail: Alexander.Demura@hepti.kiae.ru
[d] UMR 8633 du CNRS

[1] The asymptotic character of the multipole expansion of the interaction potential requires the inclusion of all terms of the same order [9]. Thus, the inclusion of quadratic Stark effect (which affects *both* the energy and the eigenstates of the radiator) has to be performed together with the second-order quadrupole effect, octupole effect, etc. [9,15].

to local microscopic departure from the average plasma quasineutrality). Moreover, the effective time scale of the process changes with the detuning from the line center. Thus, as the electron-radiator and the ion-radiator interactions have different intrinsic time scales, their influence on the line shape at the same value of detuning may differ and do not necessary cancel each other.

The aim of the present paper is to calculate the line shape with the effects of ion dynamics in the nonuniform microfield. The quadrupole radiator-plasma interaction has many-body nature: the exact theoretical treatment of the line shapes in the nonuniform microfield includes the statistical average over the ion microfield $\mathbf{F}$ and its five independent nonuniformity tensor components $\partial F_i/\partial x_k$. It is thus very complicated computationally and has never been fully performed [9–26]. A generalized self-consistent Baranger-Mozer cluster expansion method was proposed recently to construct $W(\mathbf{F};\{\partial F_i/\partial x_k\})$ – the joint distribution function of the ion microfield and of its nonuniformity tensor [11,12,15–17]. This tensor determines the value of the quadrupole part of the plasma-radiator interaction potential [10]. The adopted approach provides statistical description to all terms in the interaction potential of the same order of magnitude in the parameter $n^2a_0/Z_{\rm N}R_0$ (n – the principal quantum number, a_0 – Bohr radius, R_0 – mean distance between plasma charges, $Z_{\rm N}$ – nuclear charge of the radiator). Thus terms proportional to $\hat{R}^2{\rm div}\mathbf{F}$ are also included (where $\hat{R}^2$ is square of the electron position operator of the radiator), that were neglected before. For an ion-perturber potential screened by the plasma electrons these terms are due to the *nonuniform distribution of the electron charge cloud around the perturbing plasma ions*. That is why in [12,14–17] this part of interaction was associated with *plasma polarization*.

In practice, the theoretical treatment of the line shape, including the field nonuniformity contribution, is reduced to the calculation of the first moments of the joint distribution $W(\mathbf{F};\{\partial F_i/\partial x_k\})$ over the components of the microfield nonuniformity tensor, which can be expressed through the two universal functions $B_{\rm D}$ and $B_{\rm DO}$ [12,15, 16]. In the multipole expansion of the plasma ions-radiator interaction potential, the first function enters through a product with the traceless tensor of the quadrupole moment $\hat{Q}$. The second function $B_{\rm DO}$ is connected to the scalar part of interaction potential proportional to $\hat{R}^2$, induced by the above mentioned polarization effects. These functions were studied together in the Baranger-Mozer (BM) formalism and by Monte Carlo (MC) simulations for various plasma conditions in previous work [16,18], showing a good mutual agreement in their common range of validity. The MC approach is also considered to obtain results valid for strongly coupled plasmas.

The averaged moments of the quadrupole interaction is substituted directly in the Hamiltonian of the radiator [15,24]. The relevant statistical functions $B_{\rm D}, B_{\rm DO}$ and the field distribution function P, obtained by MC or BM methods, are used in calculations of the quasistatic profiles of hydrogen-like radiators with account of the quadrupole interaction [15,24]. The electron-radiator interaction is performed conventionally in terms of an electron relaxation operator $M(\omega)$, which in general depends on the frequency ω [28,29]. The profiles containing quadrupole effects serve as an input for the computation of the dynamic profiles in the Model Microfield Method [44,45].

The paper is organized as follows. Section 2 explains the connection between the electric microfields and the electric potentials, and the influence of the nonuniform distribution of charges. It also gives the expression for the plasma-radiator interaction potential with polarization terms. Section 3 presents the BM and MC approaches which are used for computing the universal microfield functions. Section 4 gives the basis of the line shape theory in the Model Microfield Method, which is used for the full scale calculations. In Section 5 results are given for the Lyman α line of the He^+ and Ar^{17+} ions.

2 Theory

2.1 Plasma microfields

It follows from the above analysis that the problem must be considered step by step. This is the objective of this work, which is devoted to the influence of the ion quadrupole effects on the line asymmetry, when ion dynamic effects are also taken into account. The fine structure effects and electronic shift effects will be neglected.

For simplicity we shall restrict the study to a plasma in a volume $\mathcal{V}$, consisting of identical ions, with charge Z and a hydrogenic radiating ion of nuclear charge $Z_{\rm N}$ (net charge $Z = Z_{\rm N} - 1$). The condition of quasineutrality is

$$N = N_{\rm e} = ZN_{\rm i}, \tag{1}$$

where $N_{\rm e}$ is the electron plasma density at the infinity and $N_{\rm i}$ is ionic density.

We shall denote the mean distances between the electrons and the ions by R_0 and $R_{\rm i}$ respectively.

Ions and electrons move with different time scales. This allows to consider separately for the line shape problem the ionic microfield (also called Low Frequency, LF), which is due to effective ions moving *with* a polarized electronic background, and the electronic microfield (High Frequency, HF) which is due to point charge electrons moving *on* a neutralizing ionic background. This means that the two microfield processes are statistically independent. These two pictures have been used to calculate the distribution function [30,31] of the LF microfield created by singly-ionized positive ions either on a neutral point or on an other ion of the same charge and the HF distribution function of the microfield due to electrons on a neutral point or on another electron.

The electrostatic potentials $\Phi^{(\rm i),(\rm e)}(\mathbf{r})$, created by these charges, the ionic and electronic fields, $\mathbf{F}, \mathbf{E}$, which are derived from them, their gradients and divergences are the sum of different elementary potentials $\phi^{(\rm i),(\rm e)}(\mathbf{r})$, electric

fields $\boldsymbol{\mathcal{F}}, \boldsymbol{\mathcal{E}}$..., *i.e.*

$$\Phi^{(\mathrm{i})}(\mathbf{r}) = \sum_k \phi_k^{(\mathrm{i})}(\mathbf{r}) \tag{2}$$

$$\Phi^{(\mathrm{e})}(\mathbf{r}) = \sum_j \phi_j^{(\mathrm{e})}(\mathbf{r}) \tag{3}$$

$$\mathbf{F}(\mathbf{r}) = \sum_k \boldsymbol{\mathcal{F}}_k(\mathbf{r}) \tag{4}$$

$$\mathbf{E}(\mathbf{r}) = \sum_j \boldsymbol{\mathcal{E}}_j(\mathbf{r}). \tag{5}$$

The divergence of the field is equal to the Laplacian of the electrostatic potentials and satisfies the Poisson equation, which is given for the elementary ionic and electronic potentials by

$$\Delta\phi^{(\mathrm{i})}(\mathbf{r}) = 4\pi\rho_{\mathrm{e}}(r) - 4\pi eZ\delta(\mathbf{r}) \tag{6}$$

$$\Delta\phi^{(\mathrm{e})}(\mathbf{r}) = -4\pi\rho_{\mathrm{i}}(r) + 4\pi e\delta(\mathbf{r}). \tag{7}$$

For the line shape problem, the fields are calculated at the origin of the reference frame, where the radiating atom is located. Thus $\rho_{\mathrm{i}}(r)$ in equation (7) reflects the distribution of perturber ions around this radiator ion, *i.e.* ($\rho_{\mathrm{i}}(r) = N_{\mathrm{i}}Zeg_{\mathrm{ii}}(r)$). For a neutral radiator the distribution of ionic charges in its vicinity is uniform, *i.e.* $\rho_{\mathrm{i}}(r) = N_{\mathrm{i}}Ze$. Substituting $\rho_{\mathrm{e}}(r) = N_{\mathrm{e}}eg_{\mathrm{ie}}(r)$ in equation (6), *the averages of $\Delta\Phi^{(\mathrm{i})}$ (Eq. (6)) over the positions of the perturbing ions and of $\Delta\Phi^{(\mathrm{e})}$ (Eq. (7)) over the positions of the perturbing electrons cancel each other in the Poisson equation for the averaged potential of all the plasma charges*, as expected from plasma quasineutrality and symmetry relations. One has

$$\begin{aligned}\langle\Delta\Phi^{(\mathrm{i})}\rangle &= (1/\mathcal{V})4\pi N_{\mathrm{e}}e\int g_{\mathrm{ii}}(\mathbf{r})g_{\mathrm{ie}}(\mathbf{r})\,\mathrm{d}^3r \\ &= 4\pi N_{\mathrm{e}}eB_{\mathrm{G}}.\end{aligned} \tag{8}$$

For $g_{\mathrm{ii}} = g_{\mathrm{ie}} = 1$, which corresponds to the One Component Plasma (OCP) model [32] for the electron and the ions, one finds $B_{\mathrm{G}} = 1$.

2.2 Plasma-radiator interaction

The interaction potential $\hat{V}$ between the radiator and the plasma free charges is composed of two parts, the radiator-electron interaction $\hat{V}^{(\mathrm{e})}$, and the radiator-ion interaction $\hat{V}^{(\mathrm{i})}$. For small distances R of the optically active electrons from the radiator nucleus, compared to the distances from ion perturbers, the multipolar expansion of the Coulomb interactions may be used. In terms of the total electric field of the electrons $\mathbf{E}$ and of the total electric field of ions $\mathbf{F}$, this gives to the first-order in the parameter $n^2a_0/Z_{\mathrm{N}}R_0$,

$$\hat{V} = \hat{V}_{\mathrm{D}} + \hat{V}_{\mathrm{Q}} + \hat{V}_{\mathrm{BG}} \tag{9}$$

with

$$\hat{V}_{\mathrm{D}} = -\hat{\mathbf{D}}\cdot(\mathbf{F}+\mathbf{E}) \tag{10}$$

$$\hat{V}_{\mathrm{Q}} = +\frac{1}{6}\sum_{i,j}\hat{Q}_{ij}\left(\frac{\partial F_i}{\partial x_j} + \frac{\partial E_i}{\partial x_j}\right) \tag{11}$$

$$\hat{V}_{\mathrm{BG}} = -\frac{e^2}{6}\hat{R}^2(\mathrm{div}\mathbf{F} + \mathrm{div}\mathbf{E}), \tag{12}$$

where $\hat{\mathbf{D}}$, $\hat{\mathbf{Q}}$ and $\hat{\mathbf{R}}$ are the dipole, quadrupole and position operators of the bound electron. The indices i, j... denote the Cartesian components (x, y, z) (for example $\partial F_x/\partial y$). The operator $\hat{V}_{\mathrm{BG}}$ is due to plasma polarization.

The present description of the interaction potential $\hat{V}$ between the bound electrons and the plasma presupposes the validity of the plasma microfield approach. This means that the perturbers do not penetrate inside the area of the bound electron orbits. In the case of an ionic radiator, the probability for an ion to be very close to the radiator is small, due to the Coulombic repulsion. This is not the case for the electrons, which are attracted by the net positive charge of the radiator. The treatment of these short range electron-ion interactions is beyond the scope of the present study. As a consequence, the Dirac delta functions in the equations (6, 7) for the microfields make no contribution to the line shape. Thus in the radiator-ion and radiator-electron interaction potentials in equation (12) we exclude the Dirac delta functions and denote this by the notation $\mathrm{div}'(\mathbf{F})$ and $\mathrm{div}'(\mathbf{E})$ or equivalently $\Delta'\Phi^{(\mathrm{i})}$ and $\Delta'\Phi^{(\mathrm{e})}$.

The rapidly varying electronic and slowly varying ionic fields may be considered as statistically independent. After separation of the electron and ion interactions one obtains the following expression for the ionic potential $\hat{V}_{\mathrm{BG}}^{(\mathrm{i})}$

$$\hat{V}_{\mathrm{BG}}^{(\mathrm{i})} = -\frac{e}{6}\hat{R}^2\mathrm{div}'(\mathbf{F}), \tag{13}$$

which is valid for any choice of the elementary interaction potential between each plasma ion and the radiator. Note that in the previous works, which were based on a collisional picture, $\mathrm{div}'(\mathbf{F})$ was zero because no neutralization charge was considered [9,10].

There are obvious limits to the applicability of the notion of a neutralizing static background in the context of the line shape calculations. Indeed, this will be valid for large time intervals, *i.e.* in the line centers ($\Delta\omega \ll \omega_{\mathrm{pe}}$). At sufficiently large detunings in the wings ($\Delta\omega \geq \omega_{\mathrm{pe}}$), the line shape is sensitive to the interaction with the charge which is the nearest to the radiator, regardless of its sign and of the existence of other charges. Thus in the far wings one may forget about the contributions from $\Delta\phi$, which is effectively the case. Whereas the static electron screening is, *strictly speaking*, inadequate for the full line shape calculation problem, it may be used in the line center.

As explained in the introduction, one replaces the quantities $\partial F_\alpha/\partial x_\beta$ and $\Delta\Phi^{(\mathrm{i})}$ in the expression of the line shape by their constrained averages over the field, the value of the total ionic field being fixed. This approximation, which makes it easier to calculate the line shapes, is justified by the fact that the expansion of the resolvent

up to the first-order in the constrained averages is identical with first-order perturbation theory in the line shape expression.

Thus, supposing $\mathbf{F}$ parallel to the Oz axis and replacing $\hat{D}_z$ by $-e\hat{Z}$ and $\hat{Q}_{zz}$ by $-e(3\hat{Z}^2-\hat{R}^2)$, one obtains

$$\langle \hat{V}_{\rm i}\rangle_F = e\hat{Z}F_0\beta - \frac{\pi e^2 N_{\rm e}}{3}(3\hat{Z}^2-\hat{R}^2)B_{\rm D}(\beta) - \frac{2\pi e^2 N_{\rm e}}{3}\hat{R}^2(B_{\rm DO}(\beta)-B_{\rm G}). \quad (14)$$

where $B_{\rm G}$, defined in equation (8), includes explicitly the cancellation effects of the electrons $\hat{V}^{(\rm e)}_{\rm BG}$, as discussed at the end of Section 2.1. In this equation the universal functions $B_{\rm D}(\beta)$ and $B_{\rm DO}(\beta)$ are defined by

$$\left\langle \frac{\partial F_z}{\partial z} - \frac{1}{3}\Delta'\Phi^{(\rm i)}\right\rangle_\beta = \frac{4\pi N_{\rm e} e}{3}B_{\rm D}(\beta), \quad (15)$$

and

$$\langle \Delta'\Phi^{(\rm i)}\rangle_\beta = 4\pi N_{\rm e} e B_{\rm DO}(\beta). \quad (16)$$

The scaled electric field β is given by,

$$\beta = F/F_0 \quad \text{with} \quad F_0 = 2\pi(4/15)^{2/3} e N_{\rm e}^{2/3}, \quad (17)$$

and from the equations (6–8) one verifies that

$$B_{\rm G} = \int_0^\infty {\rm d}\beta\, P(\beta) B_{\rm DO}(\beta), \quad (18)$$

where $P(\beta)$ is the field distribution function.

The values of these universal functions depend on the choice of the elementary potential $\phi^{(\rm i)}(\mathbf{r})$ between the plasma ions and the radiating ion, and on the theoretical approach to their calculation.

Due to their short time scales, the electron interaction is commonly described by a conventional electron broadening operator $M(\Delta\omega)$, calculated with the potential $\hat{V}^{(\rm e)}$. If the electronic contribution to the background has been already subtracted from the ionic one, as this is the case here, the potential $\hat{V}^{(\rm e)}$ does not include the background contribution $\hat{V}^{(\rm e)}_{\rm BG}$.

Including only the dipole part of the potential and supposing that the ionic field is static, the eigenstates of the Hamiltonian are the parabolic states $|nn_1n_2m\rangle$ with $n = n_1 + n_2 + |m| + 1$. These states are mixed together by the quadrupole effects. The relevant matrix elements are given in the Appendix.

3 Computations of the universal microfield functions

3.1 Choice of ion-radiator potential

In our numerical computation the Debye potential is used for the ion-radiator interaction. Thus one has for the elementary electrostatic ionic potential, electric fields and modified divergence (Eqs. (2–5))

$$\phi(r) = eZ\exp(-\alpha r)/r, \quad (19)$$

$$\boldsymbol{\mathcal{F}}(\mathbf{r}) = \boldsymbol{\nabla}\phi(\mathbf{r}) = -\frac{eZ\mathbf{r}}{r^3}(1+\alpha r)\exp(-\alpha r), \quad (20)$$

$$\mathrm{div}'\boldsymbol{\mathcal{F}}(\mathbf{r}) = \Delta'\phi^{(\rm i)} = eZ\alpha^2\exp(-\alpha r)/r, \quad (21)$$

where α is equal to the inverse of the electronic Debye screening length.

The average of $\mathrm{div}'\boldsymbol{\mathcal{F}}$ over the ion positions is equal to the averaged electronic screening charge of the perturbing ion weighted by the ion(i)-radiator(r) pair distribution $g_{\rm ir}(r)$

$$\int_0^\infty {\rm d}\beta\, P(\beta)\langle \Delta'\Phi^{(\rm i)}\rangle_\beta = 4\pi N_{\rm e} e\psi_{\rm ir}(\alpha) \quad (22)$$

with

$$\psi_{\rm ir}(\alpha) = \alpha^2\int_0^\infty r\,{\rm d}r\exp(-\alpha r) g_{\rm ir}(r). \quad (23)$$

Thus

$$B_{\rm G} = \psi_{\rm ir}(\alpha). \quad (24)$$

In the case of a neutral radiator, $g_{\rm ir}(r)$ is equal to unity, and one has $\psi_{\rm ir}(\alpha) = 1$. In the case of an hydrogenic radiator, $\psi_{\rm ir}(\alpha)$ is less than unity, due to the Coulomb repulsion at short distances, where $g_{\rm ii}(r)$ differs locally from unity.

3.2 Numerical Monte Carlo simulations

Numerical Monte Carlo (MC) simulation is a powerful method for studying the equilibrium states of a plasma composed of point charged particles. In a previous paper [16], we described in detail the Metropolis Monte Carlo procedure we have used, in which the originality is essentially due to the use of a spherical approximation to the potential, appropriate to the symmetry of the plasma for the plasma parameters considered [33]. The spherical approximation of the potential leads to an analytic expression for the effective binary ionic Yukawa potential, depending only on the modulus of the distance between the pair of ions. Gain in memory storage and time computing is achieved without loss of precision for microfield applications. This approximation for the potential has also been recently checked against precise Monte Carlo calculations performed on a hypersphere [34,35].

The simulations are performed in a cube with periodic boundary conditions, applying the standard Ewald procedure [36]. The particles interacts *via* Yukawa type screened ionic interaction potentials. We use the general expression for the electronic screening length, which is a temperature and density dependent Thomas-Fermi screening length [37]. This expression is valid for a wide range of plasma parameters and converges towards the Debye-Hückel limit for low correlation parameters.

MC calculations are subject to systematic errors. In order to get the maximum precision, the simulations have been performed with a large number (600) of ions. But in highly ionized dense plasmas not so many particles are required, because in that case the binary pair potentials are short ranged.

The MC code uses the Metropolis algorithm to accept and reject the configurations. Typical runs need about 100 000 representative configurations of the point ions (but often less). Thus means and histograms are achieved with $100\,000 \times 600$ samples, which is large enough for the precision needed for microfield distribution results (about 10^{-2}).

It must be noted that the chosen cell size is larger than the electronic screening length, thus preserving the quasineutrality during the simulation.

3.3 The cluster expansion

Baranger and Mozer (BM) introduced a simple cluster expansion for the Fourier transform of the microfield distribution functions and terminated the series at the second order. Other authors [38,39] have shown that this second-order BM theory agrees with Hooper's ([40,41] results for a large range of weakly correlated plasma conditions. This second-order cluster expansion method has been extended by Demura [11,12] to the joint distribution function of the field and its spatial and time derivatives. It requires the knowledge of the variations with the distance of the pair distribution functions and of the elementary electric fields, and uses the Kirkwood approximation to disentangle the triple correlations. In practice it has been applied to Debye-Hückel screened electric fields and pair distribution functions. Here the universal function B_{DO} has been calculated only to the first-order in the cluster expansion. We have performed extended comparisons with MC simulations for $P(\beta)$, B_{D} and B_{DO}. The overlap between the two methods for moderate coupling parameters and low screening gives a confidence in both computations in this density range.

3.4 Asymptotic limits

The asymptotic OCP-Nearest-Neighbor (NN) approximation for the microfield distributions and for B_{D} and B_{DO} has been already given in [16]. In the case of B_{DO}, the constant $\psi_{\mathrm{ir}}(\alpha)$ due to the background (Eq. (23)) was omitted (Eq. (54) of [16]).

It was shown that for small and moderate couplings, MC and BM converge toward the NN limit. For higher couplings, BM is no longer valid but MC converges towards the NN limit for reduced field values β of about 10. The discrepancy between exact and NN limit decreases with the coupling.

3.5 Alternative theories

The Adjustable Parameter Exponential Approximation method (APEX) has been proposed to calculate the field distribution function in the case of highly correlated plasmas and has been generalized for weakly correlated plasmas [42,43]. It is based on an independent quasiparticle model. Each of these particles produces at the test point a parameterized APEX electric field, with the inverse of the screening length given by the adjustable parameter ζ. This model has been shown to provide accurate results for the field distributions of both high and low frequency components. In this approximation, the second field moment of the distribution is expressed as a function of the fitting parameter ζ which is determined from the special exact well-known constraint on $\langle E^2 \rangle$ (see Eq. (2.13) of [42]), which gives

$$\langle E^2 \rangle(\zeta) = 4\pi N_{\mathrm{i}} kT \psi_{\mathrm{ir}}(\alpha), \tag{25}$$

where $\psi_{\mathrm{ir}}(\alpha)$ defined in equation (23). The B_{D} function has been calculated in this scheme by Kilcrease *et al.* [25]. Comparisons with MC [16] and MD [26] results show that the APEX model gives accurate results for P but is less appropriate for the field gradient calculations. More precisely, our extensive comparisons between MC and APEX results for the B_{D} function, in case of pure argon at $kT =$ 800 eV and for various densities between $N_{\mathrm{e}} = 10^{21}$ cm^{-3} and $N_{\mathrm{e}} = 10^{25}$ cm^{-3}, show large discrepancies. At small field values, this discrepancy decreases with increasing density, but is still visible at 10^{25} cm^{-3}. At large field values the discrepancy increases with increasing density. In particular, the APEX data diverge from the expected NN limit. As these large fields values have a small probability, their contribution to the line intensity and asymmetry may be not so important in the line center.

4 The line shape

The line shape and shift are determined by the interactions with the slowly moving plasma ions and the very rapidly moving free electrons. Due to these different time scales the electronic contribution to the line can be, for each value of the ionic microfield, included through a damping operator $M(\Delta\omega)$ which depends on the detuning $\Delta\omega$ from the line center. This operator $M(\Delta\omega)$ (which may have non-diagonal matrix elements) can be obtained either within quantum mechanics or using a semi-classical approximation, which means that the motions of colliding electrons are treated classically (*i.e.* with rectilinear trajectories for the electron-neutral interactions or hyperbolic trajectories for electron-ion interactions). As the line width and asymmetry are dominated by ionic effects, a semi-classical treatment of electron-radiator interaction is sufficient as a first step. Thus we shall use the semi-classical perturbative description, which is valid in the line center, as long as the detuning from line center $\Delta\omega$ is not too large compared with the electron plasma frequency ω_{pe}. The electronic contributions to the width and shift are connected to the real and imaginary parts of $M(\Delta\omega)$ respectively.

The generalized line-shape expression is given in Liouville space in terms of the Fourier transform, $\mathcal{T}(\omega)$,

of the Liouville evolution operator. Hereafter we shall denote by $|a\alpha\rangle\!\rangle$ the basis vectors of the Liouville space, where $a, b...$ are for the lower level of the transition and $\alpha, \beta...$ for the upper levels. In the present work, which is mainly devoted to the ionic contribution to the line shape, we shall use the "no quenching" approximation. This means that the ionic electric field mixes together only the states nlm with the same principal quantum number n. Thus the states $a, b, c...$ (and $\alpha, \beta, \gamma...$) are mixed together by the Coulomb potential whose expression is given in equation (14). One has for the line shape

$$\mathcal{I}(\omega) = \sum_{k,a\alpha,b\beta} r_{aa}\langle a|D_k|\alpha\rangle\langle\beta|D_k|b\rangle\langle\!\langle a\alpha|\mathcal{T}_{av}(\omega)|b\beta\rangle\!\rangle, \tag{26}$$

where $D_k = \mathbf{e}_k \cdot \mathbf{D}$ is the Cartesian component k of the dipole operator responsible for the optical transition between the states $a, b, c...$ and $\alpha, \beta, \gamma...$ The quantity r_{aa} is the statistical weight of state a, and $\mathcal{T}_{\rm av}(t)$ is the average of the evolution operator $\mathcal{T}(t)$ over all the initial positions and velocities of the plasma charges. As the states $a, b...$ are supposed to be equally populated, one can drop the term $r_{aa} = r_0$ from the line shape expression. This allows us to normalize the line profiles $\mathcal{I}(\omega)$ to

$$r_0 \sum_{a\alpha,k} |\langle a|D_k|\alpha\rangle|^2 = r_0 \sum_{a\alpha} S_{a\alpha}, \tag{27}$$

where $S_{a\alpha}$ is the usual line strength. As a consequence, the profile $\mathcal{I}(\omega)$ is normalized to unity.

The Liouville operator $\mathcal{T}(t)$ satisfies the equation of evolution:

$$\mathrm{i}\hbar\frac{\mathrm{d}\mathcal{T}(t)}{\mathrm{d}t} = \mathcal{L}\mathcal{T}(t) \quad \text{with} \quad \mathcal{T}(0) = 1, \tag{28}$$

where the Liouville operator $\mathcal{L}$ is connected to the Hilbert Hamiltonian H by

$$\langle\!\langle a\alpha|\mathcal{L}|b\beta\rangle\!\rangle = \delta_{\alpha,\beta}\langle a|H|b\rangle - \delta_{a,b}\langle\alpha|H|\beta\rangle. \tag{29}$$

The operators H and $\mathcal{L}$ are the sum of the free radiator operator H_0 (corresponding to $\mathcal{L}_0$) and the plasma-radiator interaction $\hat{V}$ (corresponding to $\hat{\mathcal{V}}$) (Eq. (14)). If the ions are fixed in space, giving a net ionic field at the radiator $\mathbf{F}$, one obtains the static evolution operator

$$\mathcal{T}_{\rm s}(\mathbf{F}) = \langle\mathcal{T}_{\rm s}(\mathbf{F})\rangle_{\rm e} = \frac{\mathrm{i}}{\pi}[\omega I - (\mathcal{L}_0 - \hat{\mathcal{V}}(\mathbf{F}))/\hbar + \mathrm{i}M(\omega)]^{-1}, \tag{30}$$

and the averaged evolution operator $\mathcal{T}_{\rm av}(\omega)$ is given in terms of the static ionic field distribution function $P(F)$ by

$$\langle\mathcal{T}(\omega)\rangle_{\rm av} = \int_0^\infty P(F)\langle\mathcal{T}_{\rm s}(\mathbf{F})\rangle_{\rm e}\,\mathrm{d}F. \tag{31}$$

It is well-established that the ion-dynamic effects have a large influence in the line center, specially for a line with a central component like Lyman α. One way to take dynamic effects into account is to use molecular dynamic simulations, with a consequent and controlled sampling of short-range interactions. We shall use here a simpler approach which consists of modeling the dynamics of the process, as explained below. The Model Microfield Method [44,45] assumes that the microfield is constant during a given time interval. The microfield then jumps instantaneously to another constant value for the next time interval. The jumping times follow Poisson statistics, with a field-dependent frequency $\nu(E)$. The calculation requires knowledge of the electronic and ionic field distribution functions. The other input parameter required is the jumping frequency $\nu(E)$, which is chosen so as to reproduce the low-density field autocorrelation function. To calculate this field autocorrelation function, we model the plasma in terms of μ ions [46] whose masses are equal to the reduced masses of the pairs (radiator-ion) and which are moving independently from each other on trajectories, that are straight lines and hyperbolas for neutral and ionized radiators respectively. The expression of the jump frequency $\nu(F)$ is taken from [46] (see also the Addenda in the present paper). This expression separates into strong field and weak field contributions, *i.e.* $\nu(F) = \nu_{\rm s}(F) + f\nu_{\rm w}(F)$. The analytical expressions for $\nu_{\rm s}$ and $\nu_{\rm w}$ are identical to those obtained for a neutral radiator. In the case of an ionic radiator, the trajectory effects are taken into account by the multiplying factor f. This factor is equal to unity when trajectory deflexions are negligible (weakly correlated plasmas or neutral radiator). The numerical value of f is numerically obtained from the estimation of the field covariance of the μ ions. This model for various correlated plasmas has been tested and discussed in several papers [47,48,50].

This model for hydrogen reproduces correctly both the line widths and the intensity profile in the line wings [49–51]. It has been applied with success to the ionic profiles and should allow us to determine the line wings, if the electronic contribution is known. This success is due to the fact that it includes, by construction, the features of the field-autocorrelation function (for the relative motions) and converges towards the static limit at high densities. Thus it performs a correct theoretical interpolation for all the line shapes between the impact regime at low density and in the line center (where the binary field-autocorrelation function is the key parameter), and the static approximation in the line wings and at high density.

The ionic MMM averaged expression of $\langle\mathcal{T}(\omega)\rangle_{\rm av}$ is given by

$$\langle\mathcal{T}(\omega)\rangle_{\rm av} = \langle\mathcal{T}_{\rm s}(\mathbf{F},z)\rangle_{\rm i} + \langle\nu\mathcal{T}_{\rm s}(\mathbf{F},z)\rangle_{\rm i} \times\langle\nu I - \nu^2\mathcal{T}_{\rm s}(\mathbf{F},z)\rangle_{\rm i}^{-1}\langle\nu\mathcal{T}_{\rm s}(\mathbf{F},z)\rangle_{\rm i}. \tag{32}$$

where $\nu = \nu(F)$ and $\mathcal{T}_{\rm s}(z)$ is the Laplace transform, at $z = \omega + \mathrm{i}\nu$, of the evolution operator calculated for a static ionic field. The angle brackets denote averages over the ionic field distribution function, so that, for example

$$\langle\nu\mathcal{T}_{\rm s}(\omega)\rangle = \int_0^\infty P(F)\nu(F)\mathcal{T}_{\rm s}(z,F)\,\mathrm{d}F. \tag{33}$$

The calculation of the operator $\langle \mathcal{T}(\omega) \rangle_{\rm av}$ in equation (32) involves the numerical inversion of the resolvent $\mathcal{T}_{\rm s}(z, F)$ due to the off-diagonal matrix elements of $\hat{V}$ and $M(\omega)$.

5 Results

We shall apply our formalism to the quadrupole asymmetry of the Lyman α line of two hydrogenic elements.

We shall first study the Lyman α line of He^+ ($\lambda_0 = 304$ Å, $\hbar\omega_0 = 40.8$ eV) for an electronic density $N_{\rm e}$ equal to 3×10^{18} cm^{-3} and a temperature $T = 20\,000$ K. The perturbers are He^+ ions. In this case, accessible for laboratory studies [52], there is strong electronic screening, with a ratio a of the electronic Debye length to the mean distance between the electrons equal to 0.76. The correlation parameter $\Gamma_{\rm i} = Z^2 e^2 / R_{\rm i} kT$ is equal to 0.2. The electronic plasma frequency $\omega_{\rm pe}$ is equal to 9.8×10^{13} rad/s, which corresponds to $\hbar\omega_{\rm pe} = 0.064$ eV. The strong field weighting parameter f of the frequency jump $\nu(F) = \nu_{\rm s}(F) + f\nu_{\rm w}(F)$ is equal to 0.92. The Doppler width is of the order of 10^{-3} eV and the broadening due to spontaneous emission decay is about 3.3×10^{-6} eV.

The second case is the Lyman α line of Ar^{17+} ($\lambda_0 = 3.75$ Å, $\hbar\omega_0 = 3306$ eV) for two values of the electronic density $N_{\rm e}$ equal to 10^{24} cm^{-3} and 10^{25} cm^{-3}. The temperature $T = 9.3 \times 10^6$ K ($kT = 800$ eV). The ionic perturbers are Ar^{17+} ions. These last conditions are typical in ICF experiments. The electronic screening is characterized by screening values a equal to 0.29 and 0.43. The correlation parameters $\Gamma_{\rm i}$ are equal to 3.3 and 7. The electronic plasma frequency $\omega_{\rm pe}$ is equal to 5.64×10^{16} rad/s and 1.78×10^{17} rad/s (which correspond to $\hbar\omega_{\rm pe} = 37$ and 117 eV). The strong-field weighting parameters f of the frequency jump is equal to 1.6 and 3.9. The Doppler width is of the order of 0.57 eV and the broadening due to spontaneous emission decay is about 0.021 eV.

The effect of the interaction $\hat{V}_{\rm BG}$ and $\hat{V}_{\rm Q}$ is to produce a shift and an asymmetry of the line. Typical parameters for the linear Stark effect, quadrupole interaction and polarization effects can be obtained for a perturbing charge at the distance $R_{\rm i}$ from the radiator which creates an electric field equal to $F_{\rm i} = Ze/R_{\rm i}^2$. The corresponding gradient is $G_{\rm i} = 2Ze/R_{\rm i}^3$. These quantities are respectively given by

$$\begin{aligned} F_{\rm i} &= 2.6 e Z^{1/3} N_{\rm e}^{2/3} \\ G_{\rm i} &= 8.4 e N_{\rm e}. \end{aligned} \tag{34}$$

One has, using the diagonal matrix elements of the dipole, quadrupole and $\hat{R}^2$ operators given in the Appendix for $n = 2, n_1 = 1, n_2 = 0$ (Lyman α line),

$$\begin{aligned} \hbar\omega_{\rm D} &= \frac{3ea_0}{Z_{\rm N}} F_{\rm i} \\ \hbar\omega_{\rm Q} &= \frac{12ea_0^2}{Z_{\rm N}^2} G_{\rm i} \\ \hbar\omega_{\rm BG} &= \frac{2\pi N_{\rm e} e^2}{3} \frac{36a_0^2}{Z_{\rm N}^2} \end{aligned} \tag{35}$$

or

$$\begin{aligned} \hbar\omega_{\rm D} &= 5.9 \times 10^{-15} Z^{1/3} Z_{\rm N}^{-1} N_{\rm e}^{2/3} \\ \hbar\omega_{\rm Q} &= 4.0 \times 10^{-22} Z_{\rm N}^{-2} N_{\rm e} \\ \hbar\omega_{\rm BG} &= 3.0 \times 10^{-22} Z_{\rm N}^{-2} N_{\rm e}. \end{aligned} \tag{36}$$

In these expressions the detunings $\hbar\omega_{\rm Q}$, $\hbar\omega_{\rm D}$, $\hbar\omega_{\rm BG}$ are expressed in eV for an electronic density in cm^{-3}. Thus the order of magnitude of the quadrupole relative to the dipole effect, and of the background relative to the quadrupole are equal to

$$\begin{aligned} \omega_{\rm Q}/\omega_{\rm D} &= 6.8 \times 10^{-8} Z_{\rm N}^{-1} Z^{-1/3} N_{\rm e}^{1/3} \\ \omega_{\rm BG}/\omega_{\rm Q} &= 0.75. \end{aligned} \tag{37}$$

One notes that the ratio of the background contribution (Eq. (18)) to the quadrupole one does not depend explicitly on the charge of the plasma ions. For our selected conditions, the relative contribution of the quadrupole is predicted to be more important for the case of argon than for the case of helium.

The line shift definition is not unique, even for a simple line, with only one maximum like Lyman α. One may, for example, take the shift of the maximum of the line or the line averaged shift. The later corresponds physically to low-resolution experiments, but it mixes the definitions of shifts and asymmetry. We shall use here the first definition, and focus more on the line asymmetry. The asymmetry parameter $A(\Delta\omega)$ is often defined as

$$A(\Delta\omega) = \frac{I(\hbar\Delta\omega) - I(-\hbar\Delta\omega)}{I(\hbar\Delta\omega) + I(-\hbar\Delta\omega)}, \tag{38}$$

where the definition of the detuning $\Delta\omega$ remains to be specified. This detuning can be measured relative to the frequency of the line in vacuum, ω_0. This definition has the disadvantage of mixing together the problems of line shift and asymmetry and requires experimentally a good comprehension of other sources of line shifts due to macroscopic motions. Thus we shall use in the following a second definition, namely the detuning $\Delta\omega$ will be taken from the position of the maximum of the line, ω_0'. We shall denote the absolute shift of the line maximum by $\Delta\omega_0' = \omega_0' - \omega_0$. The difference between the two asymmetry parameters may be seen in Figure 1.

Another description of the line asymmetry may be obtained by using the variations of the line bisector. A given intensity value normalized to its maximum $I_{\rm max}$ is obtained at two detunings, one in the red $\Delta\omega_{\rm red}$ and the other in the blue $\Delta\omega_{\rm blue}$. Thus the bisector position is defined by $\Delta\omega_{\rm bis} = 0.5(\Delta\omega_{\rm red} + \Delta\omega_{\rm blue})$.

We shall focus the discussion of the theoretical results on several points which are mainly the ion dynamic effects and the effects of $\hat{V}_{\rm BG}$ in the Hamiltonian. To calculate this background contribution, we use the universal function $(B_{\rm DO} - B_{\rm G})$, which when averaged over field is zero (see Eq. (14)). The static limit is simulated by multiplying the masses of the radiator and perturbers by a factor of 100 in the frequency jump equations. The effects

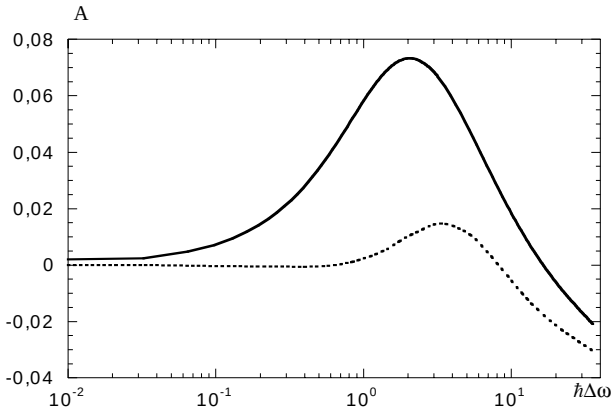

Fig. 1. Effects of the choice of the reference frequency on the asymmetry parameter $A(\Delta\omega)$, for the He^+ Lyman α line ($N_e = 3 \times 10^{18}$ cm^{-3}, $T = 20\,000$ K). The parameters obtained with reference frequency ω_0 and ω_0' are given in full and dashed lines respectively. The effect of $\hat{V}_{BG}$ is not included. The detuning $\hbar\Delta\omega$ is in units of 10^{-3} eV.

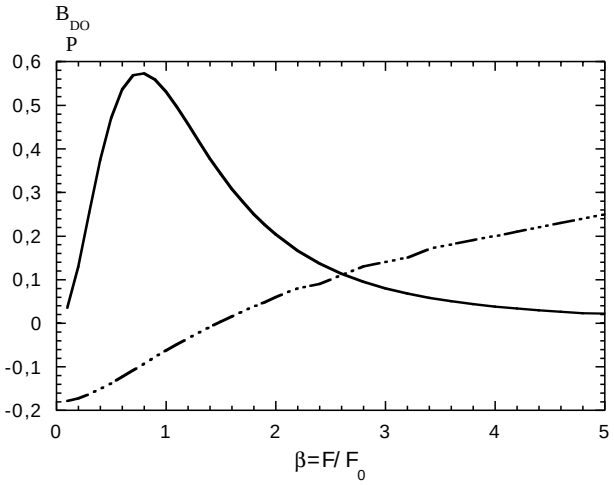

Fig. 2. Ionic microfield functions P (full line) and $(B_{DO} - B_G)$ (dotted dashed line) at an He^+ ion in function of the microfield value. The microfield is normalized to the Holtsmark value F_0, for a plasma of He^+ ($N_e = 3 \times 10^{18}$ cm^{-3}, $T = 20\,000$ K).

of the background will be tested by comparing the results including and excluding $\hat{V}_{BG}$ in the Hamiltonian.

The functions P, B_D, B_{DO} are obtained either from BM or MC calculations, depending on the case. The numerical estimations are noisy at high field values. Thus these oscillations will be smoothed out for the present line shape calculations.

The semi-classical perturbative approach, which is used to calculate $M(\omega)$, introduces a cutoff at long distances which is not too far in the line wings, that is given approximately by the minimum of the electronic Debye length and $|\Delta\omega|/\langle v\rangle$. We set the imaginary part of $M(\Delta\omega)$ equal to zero. This operator, calculated independently from the ionic microfield, is diagonal in the spherical harmonic basis. One has

$$\langle 1s0, 2lm|M(\Delta\omega)|1s0, 2l'm'\rangle = \delta_{l,l'}\delta_{m,m'}M_l(\Delta\omega). \quad (39)$$

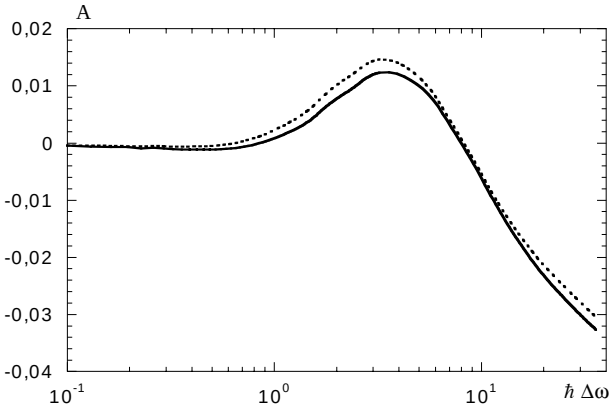

Fig. 3. Effect of the background contribution $\hat{V}_{BG}$ on the asymmetry parameter $A(\Delta\omega)$ for the He^+ Lyman α line ($N_e = 3 \times 10^{18}$ cm^{-3}, $T = 20\,000$ K). Full line, the asymmetry with background; dashed line, the asymmetry without background. The detuning $\hbar\Delta\omega$ is in units of 10^{-3} eV.

5.1 Helium Lyman α

For the selected plasma conditions the Baranger-Mozer and Monte Carlo statistical functions are in good agreement, as indicated in [16]. Thus the line shape will be calculated using BM microfield functions P, B_D and $(B_{DO} - B_G)$ (see Fig. 2 and [16] for more details). One finds $B_G = 0.95$. In the line center ($\Delta\omega = 0$), the only non zero-diagonal electronic operator elements concern the $|1s0, 2s0\rangle\rangle$ and $|1s0, 2pm\rangle\rangle$ Liouville states (Eq. (39)), $M_s(0) = 3.7 \times 10^{12}$ rad/s and $M_p(0) = 1.3 \times 10^{12}$ rad/s.

The background and quadrupole potentials have opposite signs in the Hamiltonian. Thus one expects a reduction of the quadrupole asymmetry due to the background. This, in fact, is not so obvious due to the sign changes of $(B_{DO} - B_G)$ which is negative for small field values and positive for large field values, and whose average is equal to zero (Fig. 2). We still find a reduction in the asymmetry, see Figure 3, which shows the variations of the asymmetry with and without the background contribution. The values of the line center shifts $\hbar\Delta\omega_0$ (defined as the shift of the line maximum) with and without inclusion of the background are 1.5×10^{-4} eV and 1.4×10^{-4} eV respectively. Taking B_{DO} instead of $(B_{DO} - B_G)$ leads to the much lesser red shift of -1.8×10^{-5} eV. Ion dynamic effects are known to be very important for this line, because they induce strong mixing between the central and lateral Stark components. Figure 4 indicates how the ion dynamic effects smooth the central component as compared to the static case. The halfwidth values (HWHM) are respectively equal to 2×10^{-3} eV for the dynamic case and 10^{-3} eV, for the static case. The effect on the asymmetry is illustrated in Figure 5. We note a diminution of the asymmetry due to the ion dynamic effects, see also [18,53]. The bisector variations in Figure 6 also reflect the ion dynamic effects and the effect of the background, which is more important in the static case. In the reported

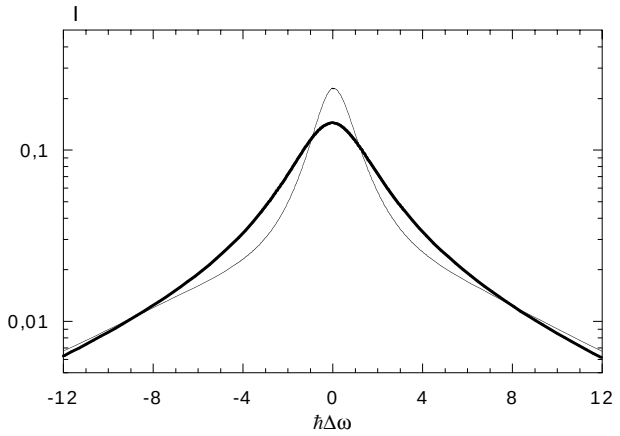

Fig. 4. Ion dynamic effects on the intensity of the He^+ Lyman α line ($N_e = 3 \times 10^{18}$ cm^{-3}, $T = 20\,000$ K). Quadrupole and background effects are included. Thick line, the dynamic profile; thin line, the static profile. The detuning $\hbar\Delta\omega$ is in units of 10^{-3} eV.

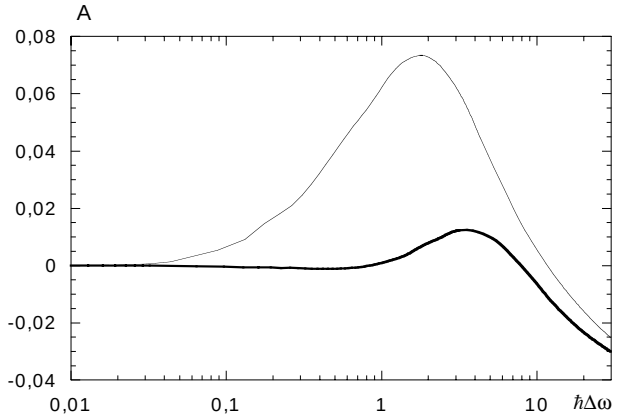

Fig. 5. Ion dynamic effects on the asymmetry of the He^+ Lyman α line ($N_e = 3\times10^{18}$ cm^{-3}, $T = 20\,000$ K). Quadrupole and background effects are included. Thick line, with ion dynamic effects; thin line, with static ions. The detuning $\hbar\Delta\omega$ is in units of 10^{-3} eV.

range of detunings, the variation of the electronic broadening operator $M(\Delta\omega)$ does not alter the results. In the case of He^+ Lyman α, Doppler broadening may affect the line center, but it is expected that it will not affect the line asymmetry. Spontaneous emission effects are negligible in the present conditions.

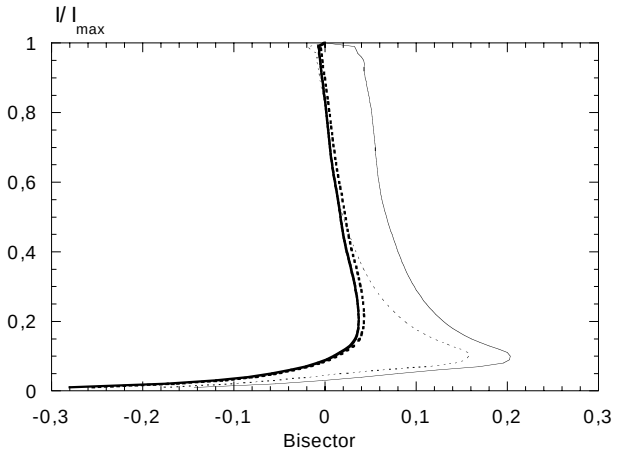

Fig. 6. Ion dynamic effects on the bisector detuning for the Lyman α line of He^+ ($N_e = 3 \times 10^{18}$ cm^{-3}, $T = 20\,000$ K). The bisector $\hbar\Delta\omega_{bis}$ and the intensity are relatively reported on x and y-axis. The intensity is normalized to the intensity maximum. The thick and thin lines are respectively used for the dynamic and static ion results. Full lines, the background is included; dashed lines, the background contribution is omitted. The detuning $\hbar\Delta\omega_{bis}$ is in unit of 10^{-3} eV.

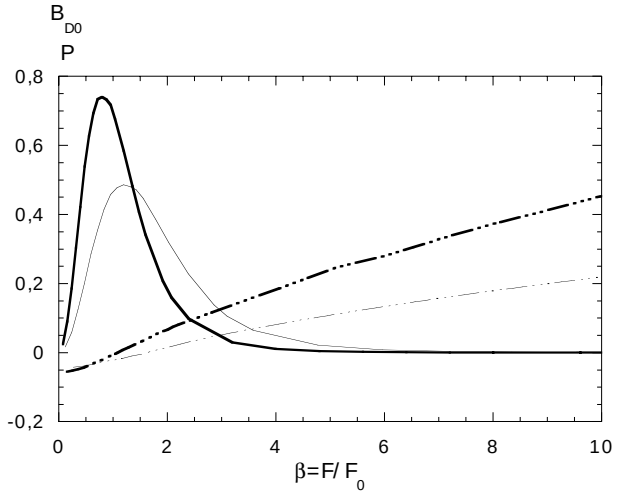

Fig. 7. Ionic microfield functions $P(\beta)$ (full lines) and $(B_{DO} - B_G)$ (dotted dashed lines), calculated at an Ar^{17+} ion, in function of the microfield value. The microfield is normalized to the Holtsmark value F_0. The plasma is composed of Ar^{17+} ions at $kT = 800$ eV and two different electronic densities $N_e = 10^{24}$ cm^{-3} (thin lines), and 10^{25} cm^{-3} (thick lines).

5.2 Argon Lyman α

The line shape will be calculated using MC field distribution functions P, B_D (see [16] for more details) and B_{DO}. The variations of $(B_{DO} - B_G)$ are reported, together with those of $P(\beta)$ in Figure 7. One has $B_G = 0.84$ and 0.7 respectively at 10^{24} and 10^{25} cm^{-3}.

In the line center ($\Delta\omega = 0$), the non-zero electronic operator elements are $M_s(0) = 7.1 \times 10^{14}$ rad/s, $M_p(0) = 2.4 \times 10^{14}$ rad/s for the low density case, and $M_s(0) = 4.4 \times 10^{15}$ rad/s, $M_p(0) = 1.5 \times 10^{15}$ rad/s for the high density case. In the "low" density case (*i.e.* at 10^{24} cm^{-3}), the values of the line center shifts $\hbar\Delta\omega_0$ with and without inclusion of the background are equal respectively to 0.081 eV and to 0.076 eV. Taking B_{DO} instead of $(B_{DO} - B_G)$ would lead to an important red shift of -0.49 eV.

In the "high" density case (10^{25} cm^{-3}), these values are equal to 0.63 eV, 0.43 eV and -4.3 eV respectively.

The background contribution seems to increase with the density as can be seen from the Figures 8 and 9.

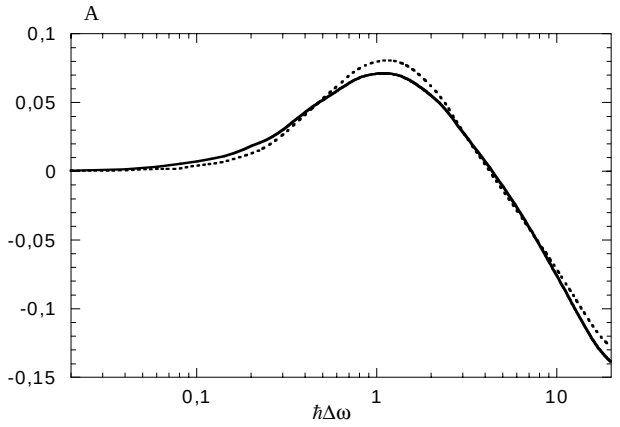

Fig. 8. Effect of the background contribution $\hat{V}_{\rm BG}$ on the asymmetry parameter $A(\Delta\omega)$ for the Ar^{17+} Lyman α line ($N_e = 10^{24}$ cm^{-3}, $kT = 800$ eV). Full line, the asymmetry with background; dashed line, without background. The detuning $\hbar\Delta\omega$ is in eV.

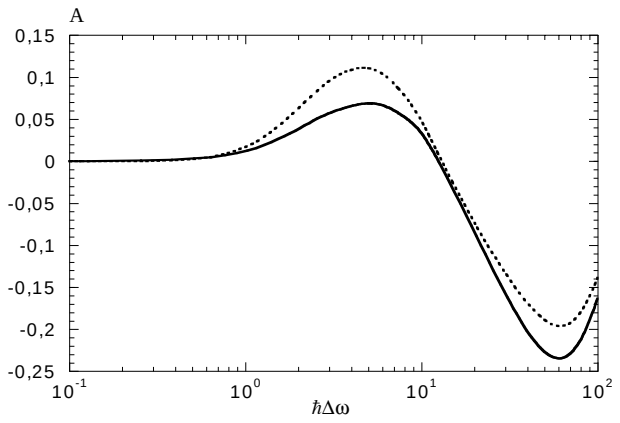

Fig. 9. Same as Figure 8 but at $N_e = 10^{25}$ cm^{-3}. The detuning $\hbar\Delta\omega$ is in eV.

The asymmetry increases strongly with the density. This is a logical consequence of the increasing contribution of short-range interactions at high densities.

The ion dynamic effects decrease with the density. These effects modify strongly the line intensity (Figs. 10 and 11). The halfwidth values (HWHM) for the static and dynamic line shapes are respectively equal to 0.23 eV and 0.60 eV at 10^{24} cm^{-3} and to 1.3 eV and 2.7 eV at 10^{25} cm^{-3}.

The ion dynamic effects are also more important at low density, as may seen from the Figures 12 and 13.

In the reported range of detunings, the variation of the electronic broadening operator $M(\Delta\omega)$ does not alter the results in the low and high density cases. As in the case of helium Lyman α, the Doppler effect plays a role in the line center, but it will preserve the relative orders of magnitude of the asymmetry parameter.

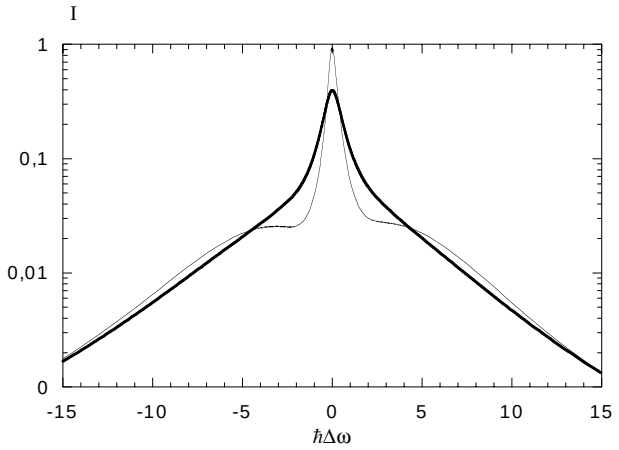

Fig. 10. Ion dynamic effects on the intensity of the Ar^{17+} Lyman α line ($N_e = 10^{24}$ cm^{-3}, $kT = 800$ eV). Quadrupole and background effects are included. Thick line, the dynamic ions profile; thin line, the static ion profile. The detunings $\hbar\Delta\omega$ is in eV and the normalized intensity in eV^{-1}.

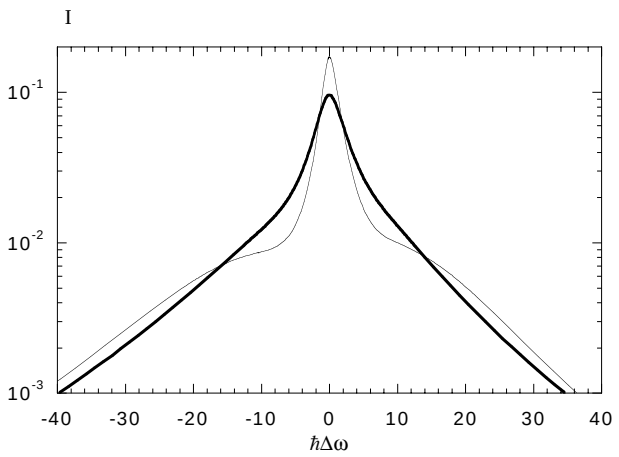

Fig. 11. Same as Figure 10 but at $N_e = 10^{25}$ cm^{-3}. The detuning $\hbar\Delta\omega$ is in eV and the normalized intensity in eV^{-1}.

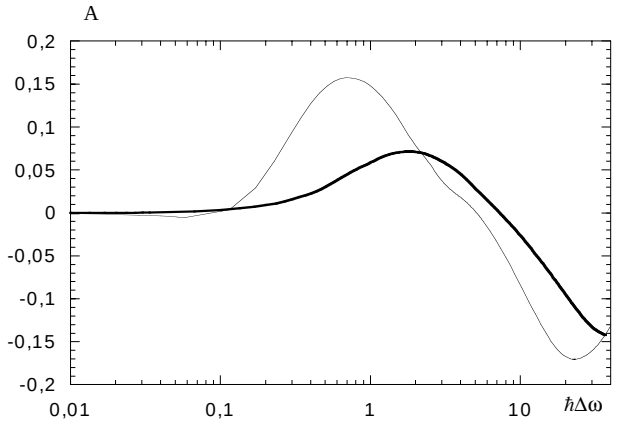

Fig. 12. Ion dynamic effects on the asymmetry of the Ar^{17+} Lyman α line ($N_e = 10^{24}$ cm^{-3}, $kT = 800$ eV). Quadrupole and background effects are included. Thick line, the static ion profile; thin line, the dynamic ion profile. The detuning $\hbar\Delta\omega$ is in eV.

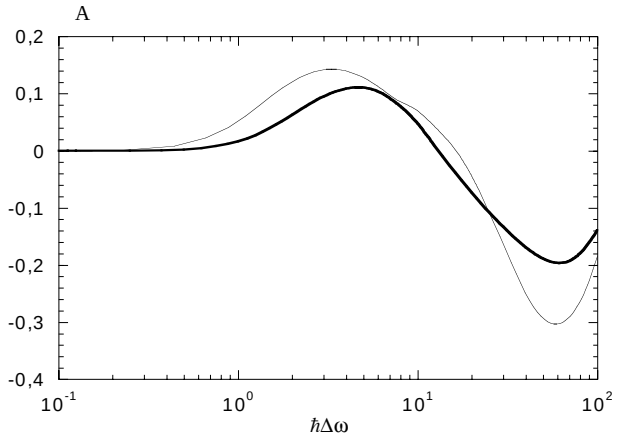

Fig. 13. Same as Figure 12 but at $N_e = 10^{25}$ cm^{-3}. The detuning $\hbar\Delta\omega$ is in eV.

6 Conclusion

The determination of the asymmetry is a very difficult task, as it is sensitive to several parameters, which in practice lead to partial cancellations in the profile. Moreover, due to its small magnitude, its numerical estimation requires very accurate line shape calculations. For the same reasons it is very difficult to propose a correct physical analysis of the experimental measurements of the asymmetry. That is why we have restricted the present study to the contributions of quadrupole terms and the associated polarization terms. We have neglected fine structure and Doppler effects and adopted a very simple description of the electronic broadening operator.

The polarization effects, considered in this paper, must be distinguished from those which arose in the connection of the "plasma polarization shift" of [5,54]. Indeed, here the plasma polarization is considered around the *pertuberions in the frame of the microfield notions, which describe distances larger than the size of the bound electron orbit.* On the contrary the "polarization shift theories" treat the interaction of plasma free electrons with the radiator, and the contribution of the penetrating collisions there is significant.

We have shown that the polarization term plays a role in the asymmetry. This contribution was omitted in the previous calculations. In the present conditions it tends to reduce the asymmetry. In the theoretical description developed here this polarization term is associated with the universal function $(B_{DO} - B_G)$ which has zero average over the field distribution function. This choice, explained in Sections 2.1 and 2.2, follows from the general consideration of the plasma quasineutrality. We have also pointed out the important role played by ion dynamics and plasma density. Our results, as noticed in [18], show that the influence of ion motion on the asymmetry is essential, in contrast to the conclusion of the papers [19,20]. Moreover, there are some unexplained differences of our results with the universal function $B_D(\beta)$ values calculated within BM formalism in [19–21].

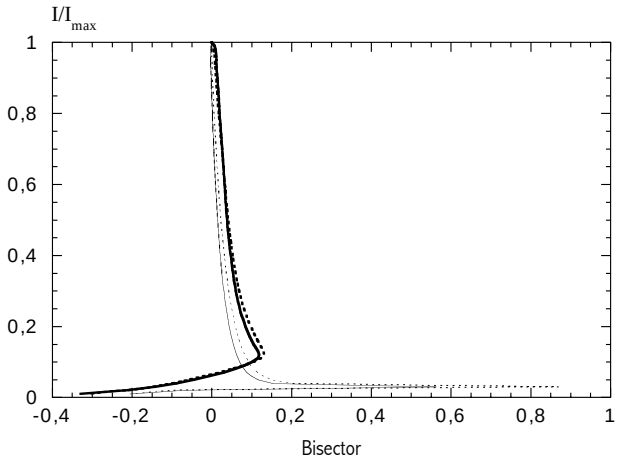

Fig. 14. Ion dynamic effects on the bisector detuning variations, for the Ar^{17+} Lyman α line of Ar^{17+} ($N_e = 10^{24}$ cm^{-3}, $kT = 800$ eV). The bisector $\hbar\Delta\omega_{bis}$ and the intensity are relatively reported on x and y-axis. The intensity is normalized to the intensity maximum. The thick and thin lines denote the dynamic and static results respectively. Full lines, the background is included. Dashed lines,the background contribution is omitted. The detuning $\hbar\Delta\omega_{bis}$ is in eV.

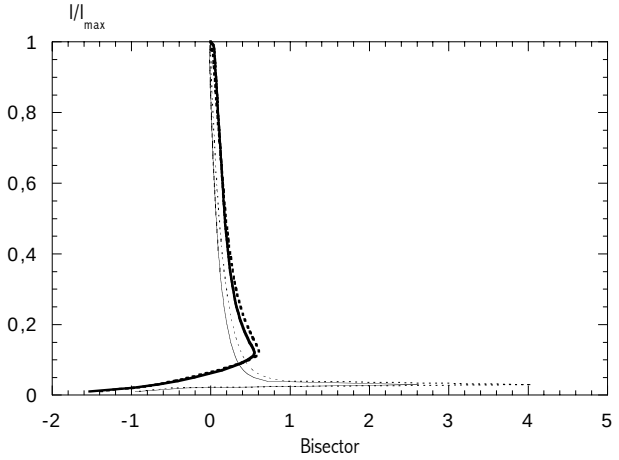

Fig. 15. Same as Figure 14 but at $N_e = 10^{25}$ cm^{-3}. The detuning $\hbar\Delta\omega_{bis}$ is in eV.

We have given all the relevant numerical quantities which may permit future comparisons with other theoretical approaches. The next step would be to include electronic contribution to the same order in the development of the Coulomb interaction potential.

The perturbative expansions of the Coulomb potential lead to convergence problems at high plasma density. That is why the molecular approach might be more suitable for some problems in strongly coupled plasmas [55], where the microfield approach can describe only a small portion of the line shape.

The authors wish to thank Dr. F. Perrot for helpful discussions and advice, and Dr. N. Feautrier for her interest, understanding and support during this work. Part of this work has been done during successive stays of Dr. A. Demura as visiting

Professor at the Paris-Meudon Observatory (DAMAP, DARC and DASGAL Departments), the support of which is gratefully acknowledged. He also acknowledges the Commissariat à l'Énergie Atomique of France and the Russian Fund for Basic Research for financial support during this study.

Appendix A: Matrix elements of Q_{zz} and R^2

The complete necessary set of the Q_{zz} and R^2 matrix elements with respect to the parabolic wave functions of hydrogen-like ions is presented below. It should prevent further disseminating errors through the literature. For example, in [19–23] the off-diagonal matrix elements of Q_{zz} are 3 times less than the correct results. In agreement with [10,14,15], one has

$$\langle n_1 n_2 m|\frac{3\hat{Z}^2-\hat{R}^2}{{a_0}^2}|n_1 n_2 m\rangle = -\frac{n^2}{Z_{\rm N}^2} \times [n^2-6(n_1-n_2)^2-1], \quad (40)$$

$$\langle n_1 n_2 m|\frac{3\hat{Z}^2-\hat{R}^2}{{a_0}^2}|n_1-1,n_2+1,m\rangle = -\frac{3n^2}{Z_{\rm N}^2} \times [(n-n_1)n_1(n_2+1)(n-n_2-1)]^{1/2}, \quad (41)$$

$$\langle n_1 n_2 m|\frac{3\hat{Z}^2-\hat{R}^2}{{a_0}^2}|n_1+1,n_2-1,m\rangle = -\frac{3n^2}{Z_{\rm N}^2} \times [(n-n_2)n_2(n_1+1)(n-n_1-1)]^{1/2}, \quad (42)$$

$$\langle n_1 n_2 m|\frac{\hat{R}^2}{{a_0}^2}|n_1 n_2 m\rangle = \frac{n^2}{2Z_{\rm N}^2} \times [2n^2+3n+3(n-1)(n_1+n_2)-6n_1n_2+1], \quad (43)$$

$$\langle n_1 n_2 m|\frac{\hat{R}^2}{{a_0}^2}|n_1-1,n_2+1,m\rangle = \frac{3n^2}{2Z_{\rm N}^2} \times [(n-n_1)n_1(n_2+1)(n-n_2-1)]^{1/2}, \quad (44)$$

$$\langle n_1 n_2 m|\frac{\hat{R}^2}{{a_0}^2}|n_1+1,n_2-1,m\rangle = \frac{3n^2}{2Z_{\rm r}^2} \times [(n-n_2)n_2(n_1+1)(n-n_1-1)]^{1/2}. \quad (45)$$

Addenda

We report a misprint in Figure 2 of [17]. The upper number on the ordinate axis should be 2 instead of the misprint 10.

The expression of the jump frequency $\nu(F)$ taken from the expressions (17, 24) of [46] is inexact. The factor $(160x)^{1/5}$ should be replaced by $(40x)^{1/5}$.

References

1. D.E. Kelleher, N. Konjevic, W.L. Wiese, Phys. Rev. A **20**, 1195 (1979).
2. J.L. Chotin, J.L. Lemaire, J.P. Marque, F. Rostas, J. Phys. B **11**, 371 (1978).
3. S. Skupsky, Phys. Rev. A **21**, 1316 (1980).
4. J. Davis, M. Blaha, J. Quant. Spectrosc. Rad. Transfer **27**, 307 (1982).
5. H. Nguyen, M. Koenig, D. Benredjem, M. Caby, G. Coulaud, Phys. Rev. A **33**, 1279 (1986).
6. A. De Kertanguy, N. Tran Minh, N. Feautrier, J. Phys. B **12**, 365 (1979).
7. O. Renner, D. Zaltzman, P. Sondhaus, A. Djaoui, E. Krousky, E. Föerster, J. Phys. B **31**, 1379 (1998).
8. G.C. Junkel, M.A. Gunderson, D.A. Haynes, C.F. Hooper, D.K. Bradley, J.A. Delettrez, P.A. Jaanimadgi, S. Regan, in *Spectral Line Shapes*, edited by R.M. Herman (AIP, New York, 1999), Vol. 10, p. 136.
9. G.V. Sholin, Opt. Spectrosc. **26**, 275 (1969).
10. A.V. Demura, G.V. Sholin, J. Quant. Spectrosc. Rad. Transfer **15**, 881 (1975).
11. A.V. Demura, thesis, Kurchatov Institute, 1976 (in *Russian*).
12. A.V. Demura, *Theory of Ion Microfield Distributions and its Spatial and Time Derivatives in Plasmas with Complex Ionisation Composition* (preprint `IAE-4632/6`, Moscow, 1988, 17p.), (in *Russian*).
13. A.V. Demura, V.V. Pleshakov, G.V. Sholin, *Atlas of Detailed Stark Countours of Hydrogen Spectral Lines in Dense Plasmas* (preprint `IAE-5349/6`, Moscow, 1991, 97p.), (in *Russian*).
14. A.V. Demura, in *Spectral Line Shapes*, edited by, R. Stamm, B. Talin (Nova Science Publ., New York, 1993), Vol. 7, p. 87.
15. A.V. Demura, C. Stehlé, in *Spectral Line Shapes*, edited by J. Drummond, A.D. May, E. Oks (AIP, New York, 1995), Vol. 8, p. 177.
16. A.V. Demura, D. Gilles, C. Stehlé, J. Quant. Spectrosc. Rad. Transfer **54**, 123 (1995).
17. A.V. Demura, Sov. Phys. JETP **83**, 60 (1996).
18. A.V. Demura, D. Gilles, C. Stehlé, in *Strongly Coupled Coulomb Systems*, edited by G. Kalman, K. Blagoev, M. Rommel (AIP, New York, 1998), p. 377.
19. S. Günter, A. Köenies, Phys. Rev. E **55**, 907 (1997).
20. M. Stobbe, S. Günter, A. Köenies, J. Halenka, J. Quant. Spectrosc. Rad. Transfer **60**, 531 (1998).
21. S. Günter, A. Köenies, J. Quant. Spectrosc. Rad. Transfer **52**, 819 (1997); *ibid* 825.
22. S. Günter, A. Köenies, Phys. Rev. E **52**, 6568 (1995).
23. J. Halenka, Z. Phys. D **16**, 1 (1990).
24. R.F. Joyce, L.A. Woltz, C.H. Hooper, Phys. Rev. A **35**, 2228 (1987).
25. D.P. Kilcrease, R.C Mancini, C.F. Hooper Jr, Phys. Rev. E. **48**, 3901 (1993).
26. D.P. Kilcrease, M.S. Murillo, L.A. Collins, J. Quant. Spectrosc. Rad. Transfer **58**, 677 (1997).
27. H.R. Griem, Phys. Rev. A **38**, 2943 (1988).
28. E.W. Smith, J. Cooper, C.R. Vidal, Phys. Rev. **185**, 140 (1969).
29. R.L. Greene, J. Quant. Spectrosc. Rad. Transfer **27**, 639 (1982).
30. B. Mozer, M. Baranger, Phys. Rev. **118**, 626 (1960).

31. M. Baranger, B. Mozer, Phys. Rev. **115**, 521 (1959).
32. M. Baus, J.-P. Hansen, Phys. Rep. **59**, 1 (1980).
33. A. Angelie, D. Gilles, Ann. Phys. Fr. Colloq. **11**, 157 (1986).
34. J.M. Caillol, J. Chem. Phys. **111**, (1999) 6528; *ibid.* **111**, 6538 (1999).
35. J.M. Caillol, D. Gilles, J. Stat. Phys. (to appear, 2000).
36. D. Gilles, *Calcul de la répartition statistique du microchamp électrique dans les plasmas*, Internal CEA-Report (1997).
37. D. Gilles, O. Peyrusse, J. Quant. Spectrosc. Rad. Transfer **53**, 647 (1995).
38. H. Pfennig, E. Trefftz, Z. Naturforsch. **21a**, 697 (1966).
39. B. Held, C. Deutsch, Phys. Rev A **24**, 540 (1981).
40. C.F. Hooper, Phys. Rev. **149**, 77 (1966).
41. C.F. Hooper, Phys. Rev. **165**, 215 (1968).
42. C.A. Iglesias, H.E. De Witt, J.L. Lebowitz, D.M. Gowan, W.B. Hubbard, Phys. Rev. A **31**, 1698 (1985).
43. J.W. Dufty, D.B. Boercker, C.A. Iglesias, Phys. Rev. A **31**, 1681 (1985).
44. A. Brissaud, U. Frisch, J. Quant. Spectrosc. Rad. Transfer **11**, 1767 (1971).
45. U. Frisch, A. Brissaud, J. Quant. Spectrosc. Rad. Transfer **11**, 1756 (1971).
46. C. Stehlé, Astron. Astrophys. **292**, 699 (1994).
47. D. Gilles, C. Stehlé, Laser Part. Beams **12**, 413 (1994).
48. D. Gilles, C. Stehlé, J. Phys. II France **5**, 75 (1995).
49. C. Stehlé, S. Jacquemot, Astron. Astrophys. **271**, 348 (1993).
50. C. Stehlé, Astron. Astrophys. Supp. Ser. **104**, 509 (1994).
51. C. Stehlé, R. Hutcheon, Astron. Astrophys. Supp. Ser. **140**, 93 (1999).
52. R. Ahmad, Eur. Phys. J. D **7**, 123 (1999).
53. A.V. Demura, D. Gilles, C. Stehlé, in *Spectral Line Shapes*, edited by M. Zoppi, L. Ulivi (AIP, New York, 1997), Vol. 9, p. 123.
54. Y. Leng, J. Goldhar, H.R. Griem, R.W. Lee, Phys. Rev. E **52**, 4328 (1995).
55. Ph. Malnoult, B. d'Etat, H. Nguyen, Phys. Rev. A **40**, 1983 (1989).